NANO LETTERS

LETTER

pubs.acs.org/NanoLett

Stochastic Sensing of Single Molecules in a Nanofluidic Electrochemical Device

Marcel A. G. Zevenbergen,[†,§] Pradyumna S. Singh,[†,‡,§] Edgar D. Goluch,[†] Bernhard L. Wolfrum,[†] and Serge G. Lemay[*,†,‡]

[†]Kavli Institute of Nanoscience, Delft University of Technology, Lorentzweg 1, 2628 CJ Delft, The Netherlands

[‡]MESA+ Institute for Nanotechnology, University of Twente, PO Box 217, 7500 AE Enschede, The Netherlands

Supporting Information

ABSTRACT: We report the electrochemical detection of individual redox-active molecules as they freely diffuse in solution. Our approach is based on microfabricated nanofluidic devices, wherein repeated reduction and oxidation at two closely spaced electrodes yields a giant sensitivity gain. Single molecules entering and leaving the cavity are revealed as anti-correlated steps in the faradaic current measured simultaneously through the two electrodes. Cross-correlation analysis provides unequivocal evidence of single molecule sensitivity. We further find agreement with numerical simulations of the stochastic signals and analytical results for the distribution of residence times. This new detection capability can serve as a powerful alternative when fluorescent labeling is invasive or impossible. It further enables new fundamental (bio)electrochemical experiments, for example, localized detection of neurotransmitter release, studies of enzymes with redox-active products, and single-cell electrochemical assays. Finally, our lithography-based approach renders the devices suitable for integration in highly parallelized, all-electrical analysis systems.

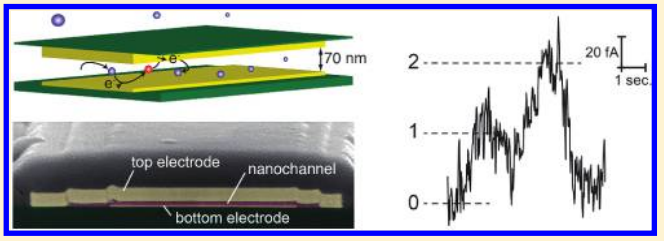

KEYWORDS: Nanofluidics, electrochemistry, single-molecule detection, redox cycling, first-passage time

The development of experimental techniques to detect and manipulate individual molecules in solution has yielded vital and unprecedented insights into molecular-scale processes, including internal dynamics, conformational changes, and intermolecular interactions.[1] These are often impossible to obtain otherwise because such information is usually averaged out when probing a macroscopic system. The most successful single molecule techniques rely on optical[2] (e.g., fluorescence[3,4]) or force-transduction[5] (e.g., optical tweezers) mechanisms, but a complementary technique based on electrical or electrochemical sensing has remained elusive.

Electrochemical detection of a single small molecule in solution at room temperature represents a formidable challenge owing to the microscopic amount of charge involved per reacting molecule. A successful approach to boost the current per molecule is redox cycling, the repeated oxidation and reduction of a target analyte at multiple electrodes, which allows each individual molecule to contribute a large number of electrons to an electrochemical current. Redox cycling is most commonly employed in scanning electrochemical microscopy (SECM), a technique which has been used to detect short-lived intermediates in electrochemical reactions,[6] image neurotransmitter release from living cells[7] and investigate the catalytic properties of surfaces.[8,9] Redox cycling has also been used to detect small numbers of molecules in closed, nanometer-high cavities formed by impinging a wax-coated metal tip onto a conducting substrate[10,11] or by immersing recessed nanoelectrodes in mercury.[12] While these experiments suggest the feasibility of single-molecule electrochemistry, practical difficulties inherent to tip-based approaches have impeded progress over the last 15 years.

The principle of operation of our device is illustrated in Figure 1a. Redox cycling takes place between two independently biased electrodes that are separated by a thin (70 nm) layer of solution. The active region of the device is defined as the volume enclosed by these two overlapping electrodes and has a length of 50 μm, a width of 1.5 μm, and a height of 70 nm. A top-view optical image and a SEM image of the cross-section of the device are shown in Figure 1b,c, respectively. In this system, the currents generated at the bottom electrode, $i_b(t)$, and top electrode, $i_t(t)$, are independently measured.

Figure 2 illustrates control experiments performed in acetonitrile (ACN) containing only 0.1 M tetrabutylammonium hexafluorophosphate ($TBAPF_6$) as supporting electrolyte. $i_b(t)$ and $i_t(t)$ exhibit only random noise with an amplitude of 7 fA rms, whether both electrodes are biased at the same potential ($E_b = E_t = -0.1$ V, Figure 2a) or at the potentials at which subsequent experiments are performed ($E_t = 0.35$ V, $E_b = -0.1$ V, Figure 2b). Since no electrochemically active species are present in the system, the observed fluctuations correspond to the background noise level of the measurement system.

Received: April 21, 2011
Revised: June 9, 2011

dx.doi.org/10.1021/nl2013423 | *Nano Lett.* XXXX, XXX, 000–000

Figure 3 shows raw current−time traces measured in the presence of 120 pM ferrocene (Fc, reduced form) as the active redox species. For this concentration of Fc, the average number of molecules present in the active region of device is given by $\langle N \rangle = CVN_A = 0.38$, where C is the bulk Fc concentration, $V = 5.3 \times 10^{-18}$ m^3 is the volume enclosed by the active region of the device and N_A is Avogadro's number. When both electrodes are biased at $E_b = E_t = -0.1$ V, no redox cycling can take place since this is a reducing potential for Fc^+ ($E^{0'}_{Fc,Fc^+} = +0.089$ V vs Ag/Ag^+) and all Fc present in the system is already in the reduced (neutral) state (Figure 3a).

In contrast, Figure 3b shows raw current−time traces measured under redox cycling conditions ($E_t = 0.35$ V, $E_b = -0.1$ V).

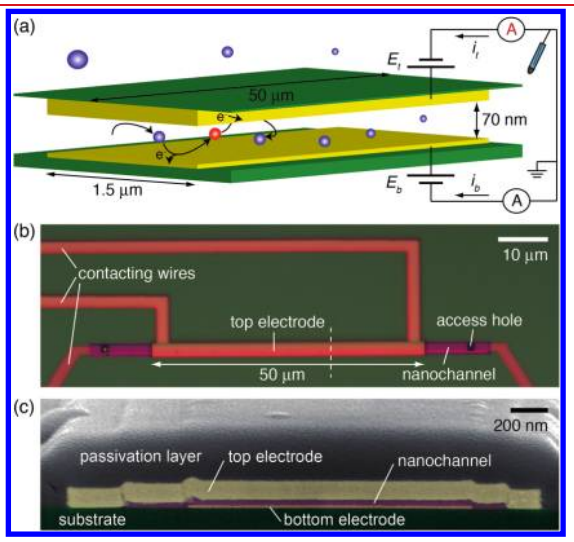

Figure 1. (a) Principle of operation of the device. Redox-active molecules undergoing Brownian motion are repeatedly oxidized and reduced at two parallel electrodes separated by a distance of 70 nm, leading to a measurable current. (b) Optical micrograph of a device (top view). Visible are the top electrode and its contacting wires (orange), the access holes (black squares), and the nanochannel connecting the active region of the device to the access holes (colored magenta for clarity). The active region of the device is connected to an outside fluid reservoir via the nanochannel, allowing the target molecules to freely diffuse between these compartments. The bottom electrode is hidden below the top electrode and the nanochannel such that only its contacting wires are visible (dark orange).The dashed white line represents the cut in (c). (c) Scanning electron microscope image of the cross-section of a device. The device was cut open using a focused ion beam.

Rapid random noise is again present in the traces. In addition, larger excursions in the current away from the baseline are observed with durations up to seconds, that is, much slower than the instrumental noise. These features occur simultaneously at the bottom and top electrodes. The sign of the current excursions is always positive at the top electrode and negative at the bottom electrode, corresponding to oxidation and reduction currents at the top and bottom electrodes, respectively. This is consistent with the oxidizing and reducing potentials applied to the electrodes. Similar features were observed in experiments with four separate devices.

We attribute the discrete features in the current to the stochastic motion of individual diffusing molecules, each event corresponding to the entry and subsequent departure of a single Fc molecule from the active region of the device. To further test this interpretation, we inverted the role of the electrodes, making the top electrode reducing and the bottom electrode oxidizing. Figure 3c shows that this causes the sign of the current excursions to be inverted, as expected if the discrete events are due to individual Fc molecules.

Figure 3d shows that for the longer events, well-defined antisymmetric plateaus in $i_t(t)$ and $i_b(t)$ are observed. In addition, shorter, smaller events are observed that are antisymmetric but do not develop into well-defined plateaus.

We first focus on the longer plateaus, which correspond in our interpretation to integer numbers of Fc molecules being present in the device. Under the simple assumption that the transport of Fc is limited by diffusion (Debye length $\ll$1 nm), the current per molecule is given by $i_p = eD/z^2$.[10] This yields $i_p = 78$ fA where $-e$ is the electronic charge, and z is the spacing between the electrodes (70 nm). Instead, the observed plateaus in Figure 3d have a magnitude $i_p = 20$ fA. We attribute this difference to adsorption of the Fc molecules to the surface of the Pt electrodes, as observed in earlier experiments.[13] Transient adsorption of Fc molecules to the electrodes leads to a decrease in i_p since diffusion between the electrodes is momentarily suspended each time that a molecule adsorbs.

Increasing the concentration of Fc is expected to lead to an increase in the average number of molecules in the device and to a corresponding increase in the size of the current excursions. Figure 4 shows a comparison of the current−time traces obtained at six different Fc concentrations. For 300 pM Fc, which corresponds to $\langle N \rangle = 0.95$, discrete steps are still discernible in the raw current−time traces but occur more frequently. For higher concentrations, changes in the instantaneous number of molecules, $N(t)$, become so frequent that they can no

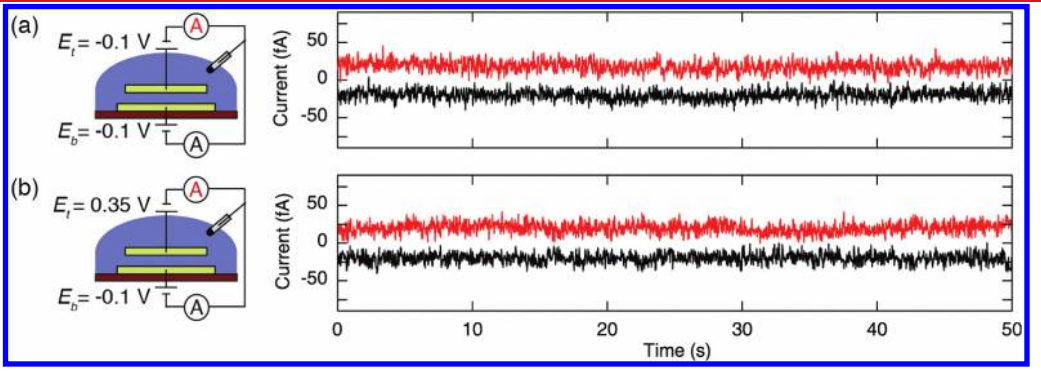

Figure 2. Control experiments in the absence of redox species. (a) Current versus time in the absence of redox species and with both electrodes set to the same bias; the traces have been vertically offset for clarity. (b) Current versus time under bias conditions that allow redox cycling.

dx.doi.org/10.1021/nl2013423 |*Nano Lett.* XXXX, XXX, 000–000

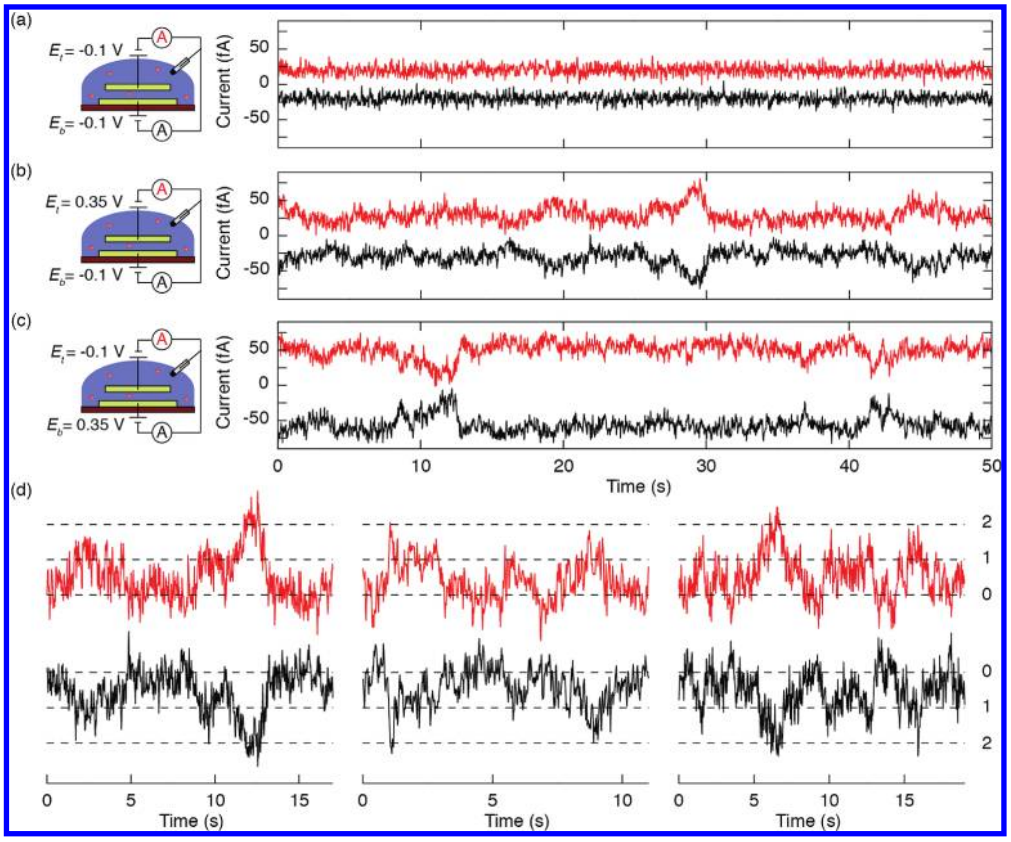

Figure 3. Raw current−time traces for an acetonitrile solution with 120 pM ferrocene as redox species and 0.1 M $TBAPF_6$ as supporting electrolyte. The current through the top and bottom electrodes are represented by the red and black solid lines, respectively; the traces have been vertically offset for clarity. (a) $E_b = E_t = -0.1$ V: No redox cycling. These traces again represent the noise level of the measurement system. (b) $E_t = 0.35$ V, $E_b = -0.1$ V: Discrete, anticorrelated fluctuations with amplitude ~20 fA are observed in both signals, each of which corresponds to an individual Fc molecule entering and subsequently exiting the device. (c) $E_b = 0.35$ V, $E_t = -0.1$ V: Each electrode now plays the opposite role (oxidation or reduction), resulting in an inversion of the polarity of the fluctuations. (d) Magnification of several long events for the same conditions as (b). During such long events the current approaches discrete current levels separated by 20 fA (dashed lines) that correspond to 0, 1, and 2 molecules being present in the device.

longer be resolved with the finite bandwidth of the measurement electronics. Figure 4 also shows histograms of the current versus time for each concentration. As the concentration is increased, the increase in the average current is accompanied by an increase in the width of the histogram. For 120 and 300 pM this spread is asymmetrically distributed, whereas it becomes increasingly Gaussian at higher concentrations.

Analysis of the stochastic signals permits an independent, quantitative test of single molecule sensitivity. For independent molecules in diffusive equilibrium with a reservoir, the number of molecules inside the active region of the device, N, is expected to follow the Poisson distribution[14]

$$P_N = \frac{\langle N \rangle^N e^{-\langle N \rangle}}{N!} \tag{1}$$

Here P_N is the probability of having N molecules inside the device at a given time. The variance of this distribution is simply equal to $\langle N \rangle$. Thus, the rms fluctuations in the number of particles, and the corresponding fluctuations in the faradaic current, are expected to scale as $\langle N \rangle^{1/2}$ or, equivalently, as $C^{1/2}$.

To test this prediction, we must first separate the faradaic fluctuations from the background noise of the measurement system. This can be achieved by performing a cross-correlation analysis of the independently measured signals at the two electrodes. These currents are given by $i_t(t) = i_{t,u}(t) + i_F(t)$ and $i_b(t) = i_{b,u}(t) - i_F(t)$, where $i_{t,u}(t)$ and $i_{b,u}(t)$ are the instrumental noise for the two detectors and $i_F(t)$ is the anticorrelated faradaic contribution to the measured currents. Noting that $i_{t,u}(t)$ and $i_{b,u}(t)$ are uncorrelated both with each other and with $i_F(t)$, it follows directly that the uncorrelated and anticorrelated parts of the fluctuations can be extracted from the simultaneously measured traces using

$$\langle i^2_{t,u}(t) \rangle + \langle i^2_{b,u}(t) \rangle = \langle (i_t(t) + i_b(t))^2 \rangle \tag{2}$$

$$\langle i^2_F(t) \rangle = -\langle i_t(t) i_b(t) \rangle \tag{3}$$

Figure 5 shows the uncorrelated and anticorrelated fluctuations as a function of C. The uncorrelated part is insensitive to C, as expected since it is caused by extraneous noise sources. Its magnitude is in agreement with the value expected from the control experiment of Figure 3a, $(7^2 + 7^2)^{1/2} = 10$ fA rms, as shown by the black line.

Similarly, the anticorrelated fluctuation level scales with $C^{1/2}$, as illustrated by the red line. This quantitative analysis therefore independently supports the conclusion that the observed discrete fluctuations originate from single molecule fluctuations.

dx.doi.org/10.1021/nl2013423 |*Nano Lett.* XXXX, XXX, 000–000

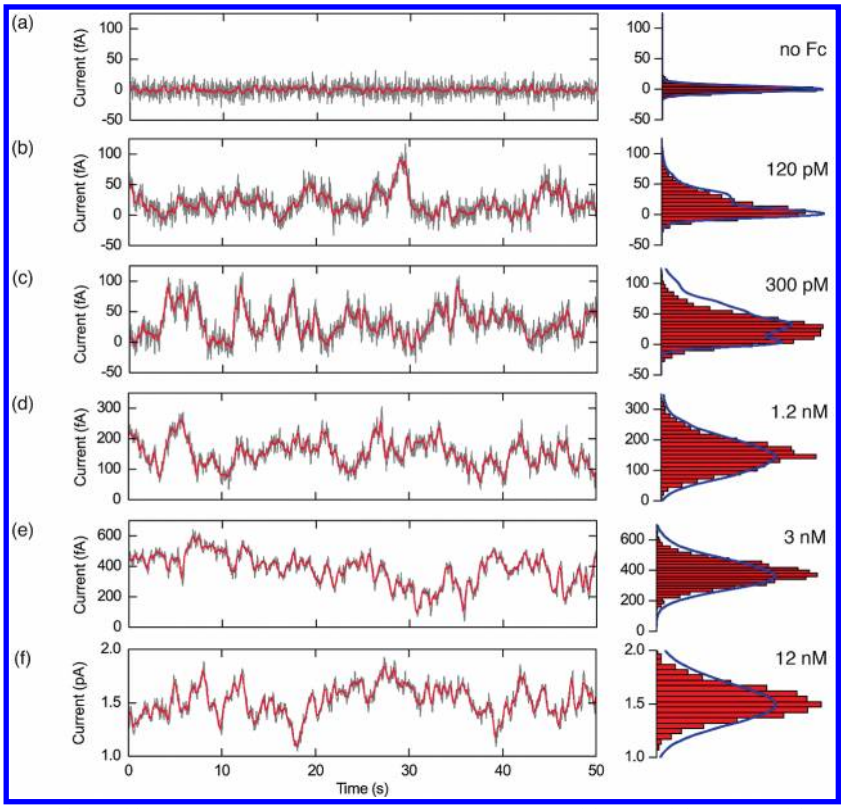

Figure 4. Current−time traces $i_t(t) - i_b(t)$ and histograms for different Fc concentrations: (a) no Fc (b) 120 pM, (c) 300 pM, (d) 1.2 nM, (e) 3 nM, and (f) 12 nM. The gray lines show the raw data while the red lines have been smoothed. Histograms of the current distribution are shown on the right; each histogram was created from at least 500 s of data. The solid blue lines are simulated histograms based on a simple random walk model, as discussed in the text.

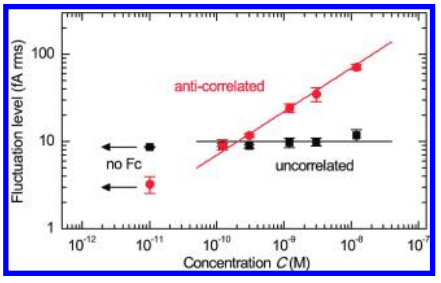

Figure 5. Uncorrelated and anticorrelated parts of the measured fluctuations in the current versus Fc concentration, C. The anticorrelated signal is proportional to $C^{1/2}$ (red line has slope =1/2), consistent with independently diffusing molecules.

In principle, one might expect to observe well-defined peaks in histograms of $i_t(t) - i_b(t)$ at values $2Ni_p$, where $N = 0, 1, 2,...$, with amplitudes given by eq 1. This is however not observed in the data of Figure 4. The apparent discrepancy originates from the space-filling property of diffusive random walks, coupled with the finite time resolution of our detection circuit. This important point is best illustrated through a comparison with simulations. We simulated molecules undergoing a random walk in a one-dimensional system. The active region between the electrodes was located in the center and represented 1% of the total system size. The remainder of the system thus played the role of reservoir. The number of molecules in the total volume was chosen such that the average number of molecules in the active region matched the concentration in the device during measurements. Following each time step, in which each random walker stepped either left or right on a lattice, the number of molecules present in the active region was determined. This led to the occupancy-time traces such as is shown in Figure 6a. Rapid telegraph-like oscillations are observed each time that a molecule is located near an edge of the active region of the device and correspond to the molecule repeatedly entering and exiting the device.

In the experiment, however, very rapid oscillations cannot be resolved due to the finite response speed of the sensitive measurement circuit (see Supporting Information). Therefore, to compare to experiments, these simulated time traces were first convolved with the measurement response function (see Supporting Information) as shown in Figure 6b. The rapid oscillations of the simulation are no longer resolved, and only the longest plateaus can be identified. The blue lines in the histograms of Figure 4 show the corresponding simulated current histograms. Notably, sharp peaks are absent in the simulated data, just as in the experiment.

Nonetheless, the simulated histograms capture the main features of the complete experimental data set for each concentration, including the absence of sharp peaks, the spread in current values and the degree of asymmetry of the distributions. Considering that the only inputs for the simulations are the concentration C, the diffusion constant D, the device volume V, the value i_p = 20 fA, and the instrument response function, all of which were independently known, this represents good agreement.

We now turn to the time duration of the events. We define the time duration of an event as the time elapsed between the entry of a randomly diffusing molecule into the active region of the

dx.doi.org/10.1021/nl2013423 |Nano Lett. XXXX, XXX, 000–000

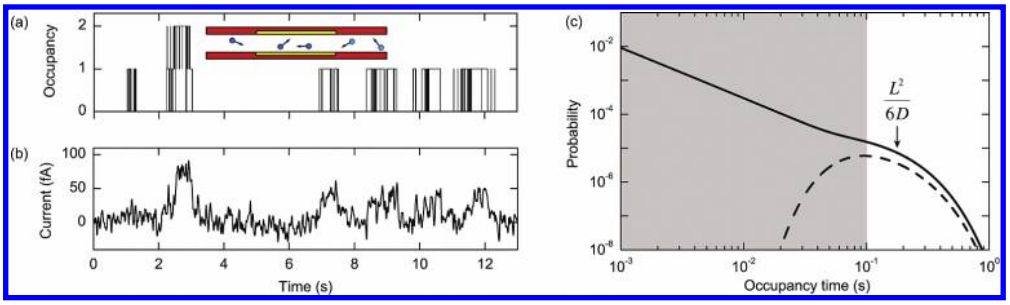

Figure 6. (a) Simulation of the number of randomly diffusing molecules present in the device as a function of time. (b) Simulated current response generated by convolving the data in (a) with measurement circuit response function and adding background noise. (c) Probability distribution of the occupancy times of a molecule in the channel. The solid curve is the probability that a molecule remains in the channel for a given occupancy time, irrespective of where it exits the channel. The dashed curve is the probability distribution of occupancy times, with the additional condition that the molecule enters from one side of the channel and exits from the other. This takes an average time of $L^2/6D$. The shaded region denotes events too short to be individually resolved in the experiment.

device and its subsequent exit. This time of first-passage corresponds to the duration of the steps we see in the current−time trace. One might intuitively expect that the average time duration of these events would be L^2/D, where L is the length of the active region of the device, times a numerical factor of order unity. However, most of the events seen in the simulated traces occur on a much faster time-scale. Why is this?

In a random walk model, a molecule entering from one side of the channel has, in principle, an infinite set of possible trajectories by which to exit on either side of the device. This multitude of trajectories spans a correspondingly wide range of durations. Determining the distribution of durations is identical to the well-known "Gambler's Ruin" problem in probability theory. The analytical solution to this problem is known[15] (see Supporting Information) and is plotted in Figure 6c. A key feature of this distribution of occupancy times, t, is that for short times it diverges as $t^{-3/2}$. This is because an event starts, by definition, when a molecule enters one end of the channel; there is thus a high probability that it leaves again from the same end after only a short time.

Figure 6c further reveals that, given the finite time response of our instrument ($\sim$ 100 ms), most of these shorter events occur on a much faster time scale than is experimentally accessible (shaded area of Figure 6c). Therefore, only the longer, much rarer, events are observed in the experiment. This highlights further why clear peaks in the histograms of both the data and the simulations in Figure 4 are not observed; most events are too short to be fully resolved, and their contribution to the measured current is heavily smoothed.

To reconcile our intuition with the predicted distribution of Figure 6c, it is useful to consider only events that correspond to entry from one end of the device and exit from the other. The distribution of durations for such events, also shown in Figure 6c, does not exhibit the $t^{-3/2}$ divergence since the molecule must travel the full distance L in this case. The mean duration of these events is given by $L^2/6D$, which is of order L^2/D as expected for a random walk.[16]

Importantly, Figure 5 indicates that concentrations as low as $\sim$100 pM can be determined from correlation analysis in these devices. This is remarkable because background currents from leakage and unwanted reactions (e.g., oxygen reduction) typically render the detection of such low concentrations practically impossible in steady-state measurements. It is possible here because the stochastic signal can be extracted from the essentially constant background current. We therefore conclude that our statistical redox cycling approach not only enhances the absolute sensitivity of electrochemical detection in terms of the number of molecules involved but also leads to important enhancements in molar sensitivity, a more significant figure of merit in many analytical applications.

The real-time detection of individual redox-active molecules as they freely diffuse in solution represents an unprecedented level of sensitivity for electrochemical fluidic sensors. While the experiments described here employed monolithic devices that were diffusively coupled to a reservoir, our microfabrication-based approach ensures that the devices can be easily incorporated into complex systems as ultrasensitive electrical sensing elements. We thus envision a wide range of applications in integrated systems for genomics, proteomics, and single-cell analysis where electrical detection may ultimately prove preferable to the currently more established optical detection techniques.

■ ASSOCIATED CONTENT

Supporting Information. Details of fabrication of nanofluidic devices, materials and methods, simulations and additional data. This material is available free of charge via the Internet at http://pubs.acs.org.

■ AUTHOR INFORMATION

Corresponding Author

*E-mail: s.g.lemay@utwente.nl.

Author Contributions

§These authors contributed equally to this work.

■ ACKNOWLEDGMENT

We thank S. W. Feldberg for suggesting the random walk model, K. Mathwig for help in determining the time response of the measurement circuit, A. J. Bard, C. Dekker, and P. K. Mandal for useful discussions, and NanoNed and NWO for financial support.

■ REFERENCES

(1) Walter, N. G.; Huang, C.-Y.; Manzo, A. J.; Sobhy, M. A. *Nat. Methods* **2008**, *5* (6), 475–489.

dx.doi.org/10.1021/nl2013423 |*Nano Lett.* XXXX, XXX, 000–000

(2) Moerner, W. E. *Proc. Natl. Acad. Sci. U.S.A.* **2007**, *104* (31), 12596–12602.
(3) Schmidt, T.; Schütz, G. J.; Baumgartner, W.; Gruber, H. J.; Schindler, H. *Proc. Natl. Acad. Sci. U.S.A.* **1996**, *93* (7), 2926–2929.
(4) Weiss, S. *Science* **1999**, *283* (5408), 1676–1683.
(5) Neuman, K. C.; Nagy, A. *Nat. Methods* **2008**, *5* (6), 491–505.
(6) Bi, S.; Liu, B.; Fan, F.-R. F.; Bard, A. J. *J. Am. Chem. Soc.* **2005**, *127* (11), 3690–3691.
(7) Schulte, A.; Nebel, M.; Schuhmann, W. *Annu. Rev. Anal. Chem.* **2010**, *3* (1), 299–318.
(8) Rodríguez-López, J.; Alpuche-Avilés, M. A.; Bard, A. J. *J. Am. Chem. Soc.* **2008**, *130* (50), 16985–16995.
(9) Bard, A. J. *J. Am. Chem. Soc.* **2010**, *132* (22), 7559–7567.
(10) Fan, F. -R. F.; Bard, A. J. *Science* **1995**, *267* (5199), 871–874.
(11) Fan, F. -R. F.; Kwak, J.; Bard, A. J. *J. Am. Chem. Soc.* **1996**, *118* (40), 9669–9675.
(12) Sun, P.; Mirkin, M. V. *J. Am. Chem. Soc.* **2008**, *130* (26), 8241–8250.
(13) Zevenbergen, M. A. G.; Singh, P. S.; Goluch, E. D.; Wolfrum, B. L.; Lemay, S. G. *Anal. Chem.* **2009**, *81* (19), 8203–8212.
(14) Bard, A. J.; Fan, F.-R. F. *Acc. Chem. Res.* **1996**, *29* (12), 572–578.
(15) Feller, W. *An Introduction to Probability Theory and its Applications*, 3rd ed.; John Wiley & Sons: New York, 1968; Vol. 1.
(16) Redner, S. *A Guide to First-Passage Processes*; Cambridge University Press: Cambridge, U.K., 2007.

dx.doi.org/10.1021/nl2013423 |*Nano Lett.* XXXX, XXX, 000–000